

Convolutional Neural Network for Classifying the Stages of the Cell Cycle

Edgar F. Duque-Vazquez^{1,1}, Jonathan Cepeda-Negrete^{2,2†},
Joel E. López-Meza^{3,3†}, Noe Saldana-Robles^{4,1†},
Raul E. Sanchez-Yanez^{1,1*†}

¹Department of Agricultural Engineering, Universidad de Guanajuato, Ex Hacienda El Copal km 9; carretera Irapuato-Silao; A.P. 311, Irapuato, 36500, Guanajuato, Mexico.

^{2*}Department of Electronics Engineering, Universidad de Guanajuato, Carretera Salamanca - Valle de Santiago km 3.5 + 1.8 Comunidad de Palo Blanco, Salamanca, 36885, Guanajuato, Mexico.

³Centro Multidisciplinario de Estudios en Biotecnología de la facultad de Medicina Veterinaria y Zootecnia, Universidad Michoacana de San Nicolas de Hidalgo, Km 9.5 Carretera Morelia-Zinapécuaro, Posta Veterinaria, Morelia, 58893, Michoacan, México.

*Corresponding author(s). E-mail(s): sanchezy@ugto.mx;
Contributing authors: ef.duquevazquez@ugto.mx; j.cepeda@ugto.mx;
elmeza@umich.mx; saldanar@ugto.mx;

[†]These authors contributed equally to this work.

Abstract

The cell cycle represents a highly coordinated process, the improper regulation of which can trigger diseases such as cancer. The detailed observation of the cell cycle constitutes a fundamental starting point for the diagnosis and prevention of diseases, while simultaneously paving the way for computational approaches, solidifying them as tools that contribute to a more precise and effective observation. Nevertheless, existing tools often manifest a propensity for errors. In this context, the present study is directed towards methodological improvement by introducing a convolutional neural network model designed to achieve a more precise classification of cell cycle states. The developed convolutional neural network model underwent a thorough comparison with models designed by other researchers who also addressed the classification of cell cycle stages using similar

datasets. The results revealed that the proposed model demonstrated a notable ability to classify the various phases of the cell cycle. With a weighted average of 93.72% using the F1 metric, it significantly outperformed models previously documented by other authors in similar research studies. The developed model demonstrated greater consistency with the inherent characteristics of the data used, resulting in a more accurate classification of cell cycle stages. This outcome underscores the distinctive ability of a convolutional neural network to identify patterns in the cell cycle more precisely than human perception, which, at times, may be susceptible to errors.

Keywords: jurkat cells, machine learning, imbalanced, cancer

1 Introduction

The cell cycle is a highly coordinated process that encompasses two general states: interphase and mitosis. Each of these states is divided into specific phases. The interphase is subdivided into G1, S, and G2, in that order. Mitosis, on the other hand, is divided in prophase, metaphase, anaphase, and telophase [1].

In the study of a cell, the analysis of the cell cycle is of great significance. Inadequate regulation of the cell cycle can lead to cell abnormalities, which, in turn, may contribute to the development of diseases such as cancer [2]. These abnormalities can be prevented and diagnosed through the observation and analysis of each of the cell cycle states.

The alterations in cellular morphology during the various phases of the cell cycle tend to be ambiguous from a visual perspective. In this context, we provide a brief explanation of the events that occur in each phase, as well as the magnitude of the visible transformations in cellular morphology in a subsequent moment.

The morphology of a cancerous cell displays variability with respect to its state in the cell cycle. During the initial phase of the cell cycle, known as G1, the cell undergoes protein and ribonucleic acid (RNA) synthesis. In this period, the cell maintains a constant morphology. The S phase constitutes the second stage of the cell cycle. At this point, the cell initiates morphological changes, exhibiting irregular shapes and undergoing an increase in size. During the third phase, known as G2, the cell initiates the duplication process of its organelles, leading to significant morphological changes compared to the two preceding phases of the cell cycle. In the prophase and metaphase stages, which belong to mitosis, no visible morphological differences are observed at a glance compared to the G2 phase. In the anaphase, notable differences become evident as the cell initiates the process of separation into two daughter cells. In the telophase, preceding cytokinesis, the cell is practically divided into two new cells, resulting in a visually evident morphological change [3].

The observation of cell alterations is carried out through microscopy techniques. The most commonly used methods in cell cycle analysis range from the use of flow cytometry [4] to the calculation of DNA content in the cell [5]. Biomarkers, such as FUCCI technology [6] are also utilized. However, it is important to note that the

mentioned techniques do not provide extensive details about cell morphology in each phase of the cell cycle [7].

Currently, data analysis plays a pivotal role in virtually all areas of research. In the study of the cell cycle, it is no exception, as the application of computer vision techniques or machine learning enables the classification of cell cycle phases through images. The use of deep learning networks is the most commonly employed tool when it comes to cell cycle phase classification.

Abin et al. [8], utilized a Recurrent Neural Network in combination with Convolutional Gated Recurrent Unit layers in two of their works for cell cycle classification [8]. Both studies, a comparison was made with a ResNet model [9].

Narotamo et al. [6], uses FUCCI technology as an indicator to determine the cell cycle phase. In their work, they emphasize the use of the DAPI compound, which is employed for identifying the cell nucleus, particularly in cell cycle studies. In their cell cycle analysis studies, they employed a Support Vector Machine (SVM) for phase classification. Additionally, in another study [10], they proposed three approaches based on the Fast YOLO algorithm and the use of the DAPI compound for cell staining, primarily for classifying phases corresponding to the cell cycle interphase. On another note, Rappez et al. [11], created a deep neural network called DeepCycle to reconstruct the cell cycle trajectory. In this approach, as in previous works of them, they employed FUCCI technology.

The methodology proposed in this work is situated within a broader context and is closely related to various previous studies, especially concerning the employed dataset. In order to emphasize the current contributions in the field, the following works are presented in chronological order.

Eulenberg et al. [12] conducted the reconstruction of the cell cycle with the purpose of elucidating its behavior in the progression of diabetic retinopathy. For this, they implemented a neural network called DeepFlow based on MXNet, through which they classified the different states of the cell cycle, achieving an accuracy of 79.40% considering the seven states of the cycle. However, in some phases, the algorithm's classification proved to be deficient due to the limited number of available images [12].

Jin et al. [7], introduced the use of the WGAN-GP data augmentation technique to mitigate the issue of data imbalance, particularly in the phases of cell division. Subsequently, they implemented a ResNet-41 model. Considering the classification of the seven phases, they reported an accuracy of 82.10%.

Rana et al. presented two studies in which they classified the cell cycle [13][14]. Similar to Jin et al., they addressed the issue of data imbalance by employing a combination of two data augmentation techniques: WGAN and mixup. In their results, they achieved an accuracy of 85%. In their second study, they combined three data augmentation techniques: WGAN, mixup and nonlinear mixup resulting in an accuracy of 85.6% .

Despite the use of data augmentation techniques in each of the articles presented, the issue of low classification results in each of the cell cycle phases, especially during mitosis, still persists. In this work, we introduce an algorithm capable of classifying the phases of the cell cycle with higher accuracy than the aforementioned algorithms.

The article is divided into four sections following this introduction. In the next section, we will discuss the methodology used. Subsequently, the results will be introduced through images and graphs, along with their discussion. Finally, we will present the conclusions reached at the end of this study.

2 Methodology

In this section, the methodology employed in the development of the proposed CNN model in this study is outlined. Firstly, the details of the dataset used are presented. Subsequently, the architecture of the developed CNN model is described in detail. Finally, a concise explanation of the methods with which we conducted comparisons is provided, along with a description of the functioning of the metrics used to evaluate the performance of the developed model.

In a general sense, the Figure 1 illustrates the procedure followed for the development of the proposed model in order to assess its performance compared to methodologies of other authors, data augmentation techniques were employed to gain a differentiated perspective on the proposed model. The detailed methodology is presented below.

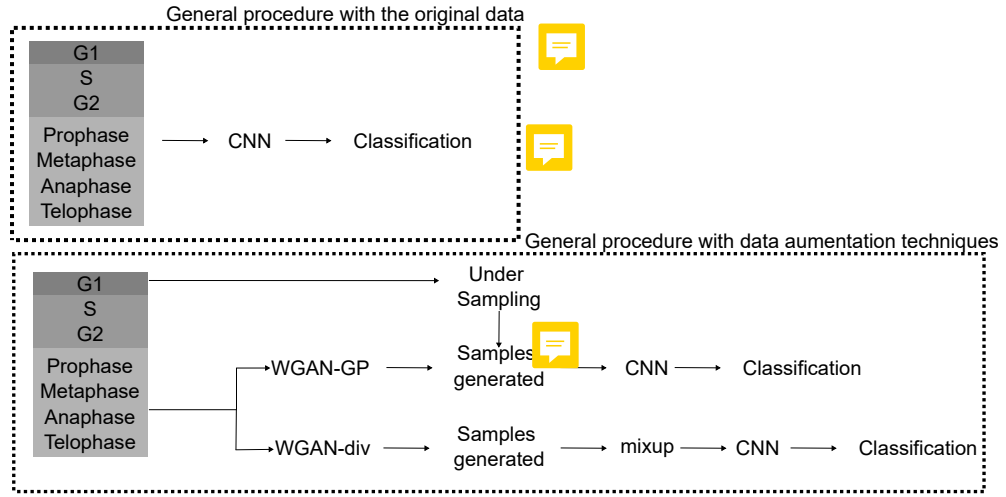


Fig. 1: The general procedure carried out in this work.



Target
Area 2

2.1 Dataset

The dataset used was extracted from the work of Eulenberg et al [12]. This dataset comprises four channels (brightfield, darkfield, and fluorescence channels), each with 32,266 images. These images correspond to cancer cells from the Jurkat cell line and were captured through imaging flow cytometry. There are two yellow speech bubble icons next to this section.

In our study, the brightfield and darkfield channels were used. The dataset is divided into seven classes (states), corresponding to the phases of the cell cycle: G1, S, G2 (interphase), and Profase, Metafase, Anafase, and Telofase (mitosis). The distribution of images per class is shown in Figure 2. The images have a size of 66x66 pixels and are in color format.

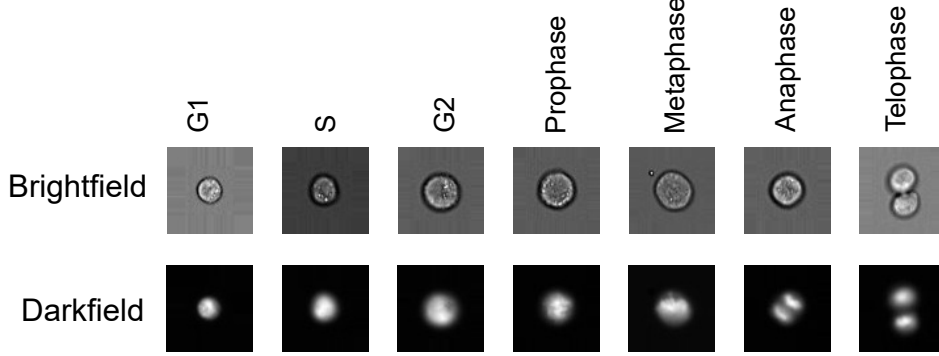


Fig. 2: Example of images of the cell cycle arranged by phase, employed in this study.

2.2 Developed CNN model

Given the specific characteristics of the data, a Convolutional Neural Network (CNN) model has been designed, following standard conventions in the field. The model consists of two convolutional layers, each followed by a max-pooling layer. The convolutional layers are configured with kernels of 64 and 32, which learn the features of the image. The kernel sizes are 10 and 5, respectively. The activation function used in each of these layers is the Rectified Linear Unit (ReLU).

Subsequently, the flattening technique was implemented and connected to a dense layer composed of 32 neurons, followed by a dropout layer to mitigate the risk of overfitting. Then, another dense layer with 16 neurons was used; in both dense layers, the ReLU activation function was applied. Finally, a dense layer with 7 neurons was incorporated, each representing one of the cell cycle states to be classified. Consequently, a softmax activation function was applied to the last layer, facilitating the classification of the different categories (see Figure 3).

2.3 Training model

The network was trained with the dataset mentioned in the methodology, which was split into two sets: training data (80% of the images) and test data (20% of the images). The model was compiled using a categorical cross-entropy loss function, commonly employed in multiclass classification problems. The Adam optimization function was used with a learning rate of 0.0001, $\beta_1=0.9$, and $\beta_2=0.999$, along with a batch size of 32. Finally, accuracy was employed as a metric to assess the model's performance during both training and evaluation.

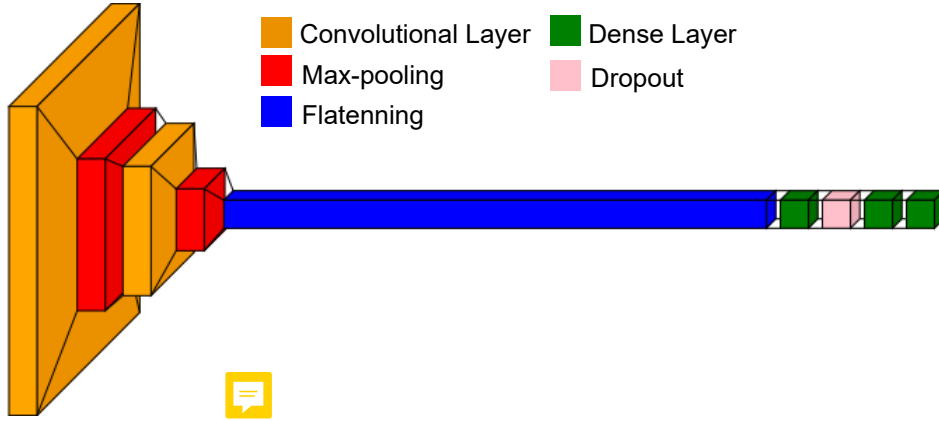


Fig. 3: Built Convolutional Neural Network Architecture

The dataset used exhibited data imbalance in the phases corresponding to mitosis, posing a potential overfitting problem during training. To address this, the authors who utilized the same dataset chose to employ data augmentation techniques to achieve a balance in the amount of data per class. The data augmentation techniques used were WGAN-GP [15] and WGAN-div [16] in combination with *mixup* [17]. These techniques are explained in detail below.

2.4 Development of other methodologies

Based on the methodology of [7], the data augmentation technique was employed. The network was trained using a batch size of 4 for Anafase and Telofase, and 16 for Metafase and Profase. Training was carried out for 7000 epochs, with a learning rate of 0.00001, $\beta_1 = 0.01$ and $\beta_2 = 0.999$. The size of the images was adjusted from $66 \times 66 \times 3$ to $64 \times 64 \times 3$. The network hyperparameters were kept at their default values. This was done to achieve a balance between the mitosis classes and the interphase classes. However, the G1 class had an excess of samples, so undersampling was applied by randomly removing images from the G1 phase.

With the new data set ready, the model developed in Section 2.2 was trained with the newly assigned hyperparameters, obtaining new performance values for the classification of cell cycle states.

Similarly, based on the methodology of Rana et al., the data augmentation technique WGAN-div was used in combination with the *mixup* technique. The batch size for all classes was 64, while the learning rate was 0.0001 for Profase, Metafase and Anafase, and 0.00001 for Telofase, $\beta_1 = 0.01$ and $\beta_2 = 0.999$. Like WGAN-GP, the size of the images was adjusted from $66 \times 66 \times 3$ to $64 \times 64 \times 3$. The number of training steps for the discriminator per iteration was 10 for Profase and 4 for Metafase, Anafase and Telofase. The network hyperparameters were kept at their default values. Half of the images obtained by WGAN-GP had the *mixup* technique applied and were combined with the images obtained by WGAN and the original images. With

this new dataset, the model developed in Section 2.2 of this chapter was trained with the hyperparameters initially assigned.



2.3 F1-Score

The F1-score metric is commonly employed in the evaluation of classification models, as it combines two key metrics: precision and recall. The standard practice involves using these metrics together to provide a comprehensive assessment of the model's performance. F1 reaches its optimal value at 1 and its minimum at 0 [18]. The F1 score is calculated using the Formula 1.

$$F1 = \frac{2 \cdot (Precision \cdot Recall)}{(Precision + Recall)} \quad (1)$$

where F1 is given by 2 and 3

$$Precision = \frac{TruePositives}{TruePositives + FalsePositives} \quad (2)$$

$$Recall = \frac{TruePositives}{TruePositives + FalseNegatives} \quad (3)$$



3 Results

The presented work introduces a convolutional neural network (CNN) model designed to classify the different phases of a cancerous cell cycle. This model was trained using images from the Jurkat cell line. To validate the efficiency of the developed model, a comprehensive comparison was conducted between the obtained results and those of other deep learning models utilizing the same database, as detailed in the introduction and methodology of the work. The selected metrics for model evaluation include precision, recall, the F1 score, and the weighted average of the F1 score. It is crucial to note that, during the evaluation of the proposed model, a 5-fold stratified cross-validation was employed. In this section, the evaluation and discussion are divided into two parts: the first regarding the dataset without modifications, the second concerning the data set with data augmentation using the WGAN-GP and WGAN-div + mixup techniques.



Evaluation of CNN on original data

In this study, the adoption of a Convolutional Neural Network (CNN) was based on several considerations. The utilization of a CNN is characterized by reduced complexity and heightened suitability, primarily owing to the available volume of data, which aligns seamlessly with the requisites of a moderately deep network. Furthermore, the deployment of a CNN is associated with reduced computational overhead and faster data processing.

The magnitude and heterogeneity of the training dataset constitute pivotal determinants for the efficacy of the developed model. In particular, for classes G1, S and G2, a substantial volume of data facilitates the assimilation of common patterns by

the model. However, the remarkable resemblance observed among images from distinct classes presents a challenge to the model’s classification accuracy, particularly concerning class S. This intricacy is discernible in the confusion matrix illustrated in Figure 4, in which the model exhibits a propensity to misclassify class S as G1 and G2, thereby contributing to a reduction in overall model accuracy. Conversely, the classes associated with mitosis exhibit a significant scarcity of images in both the training and validation sets. This data limitation adds an additional level of complexity to the model’s task, as it fails to adequately grasp the specific patterns inherent in these categories.

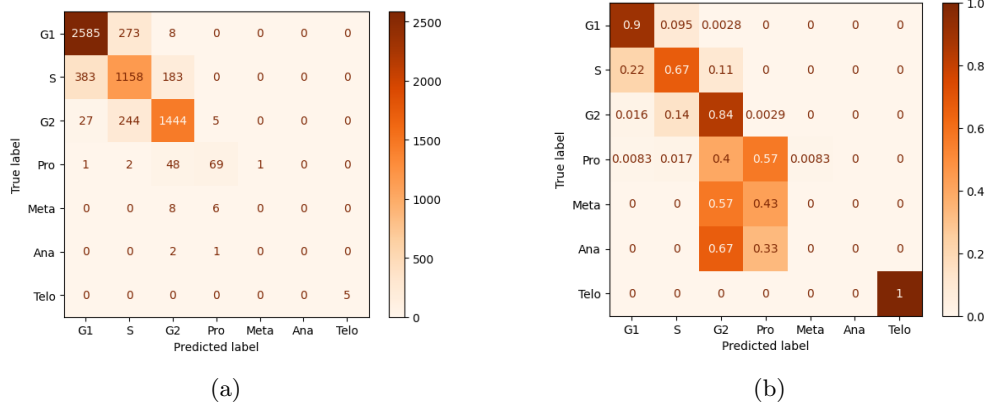


Fig. 4: a) Confusion matrix of the classification of the dataset without modifications. b) Confusion matrix normalized of the classification of the dataset without modifications.

Due to inherent characteristics in the employed data, such as the disparity in the number of samples per class and the overall dataset size, the neural network tends to experience overfitting in those classes with higher representation, leading to poor performance and directly impacting the overall model performance, as illustrated in Figure 5. Model training was halted at epoch 22, considering the observed variations in the loss function on the validation data. In this figure, an increase in the loss function of the validation data is evident, contrary to expectations, and a decrease in accuracy is observed instead of an improvement.

In order to assess the performance of the proposed model, a detailed comparison was conducted, as illustrated in Table 1, between the outcomes achieved by our model and those obtained by Jin et al. In this table, it becomes evident that the imbalance in the distribution of data per class emerges as a determining factor in the model’s performance.

Positive outcomes stand out in the G1, G2, and Telophase stages, largely attributable to the abundance of data and the clarity of the object to be classified in the images, in contrast to other phases of the cell cycle. The metrics reveal a significant difference favoring our model compared to that developed by Jin et al.



Fig. 5: The train and validation accuracy and the train and validation loss of the model proposed.

This analysis highlights the crucial importance of managing the imbalance in the quantity of data per class to enhance the model's generalization. The quality and quantity of available data are fundamental elements that directly impact the model's ability to effectively classify the various phases of the cell cycle.

Table 1: Comparison of the classification results between our model and those of Jin et al., using the original dataset.

Phase	Precision		Recall		F1	
	Jin et al.'s model	Proposed model	Jin et al.'s model	Proposed model	Jin et al.'s model	Proposed model
G1	0.8316	0.8628	0.8403	0.9020	0.8359	0.8820
S	0.6765	0.6905	0.7052	0.6717	0.6905	0.6810
G2	0.8453	0.8529	0.8012	0.8395	0.8241	0.8462
Prophase	0.8521	0.8519	1.0000	0.5702	0.9202	0.6832
Metaphase	0.0000	0.0000	0.0000	0.0000	0.0000	0.0000
Anaphase	0.0000	0.0000	0.0000	0.0000	0.0000	0.0000
Telophase	0.0000	1.0000	0.0000	1.0000	0.0000	1.0000
Weighted Average	0.7835	0.8117	0.7844	0.8152	0.7853	0.8127

3.1 Results of the CNN architecture trained with data augmentation techniques

To address the data imbalance, Jin et al., proposed the implementation of the WGAN-GP data augmentation technique, coupled with undersampling in the G1 phase. The methodology of by Jin et al. was adopted to assess the performance of the proposed CNN model, now incorporating data augmentation techniques.

Figure 6 displays the depicting results in a confusion matrix of the model trained with data augmentation and G1 undersampling. Recalling the challenges encountered with imbalanced data, an increase in the number of true positives in class S is observed, while the count of true negatives and false negatives has slightly decreased. Furthermore, in states associated with mitosis, a notable increase in true positives is evident, a consequence of incorporating new data provided by the data augmentation technique.

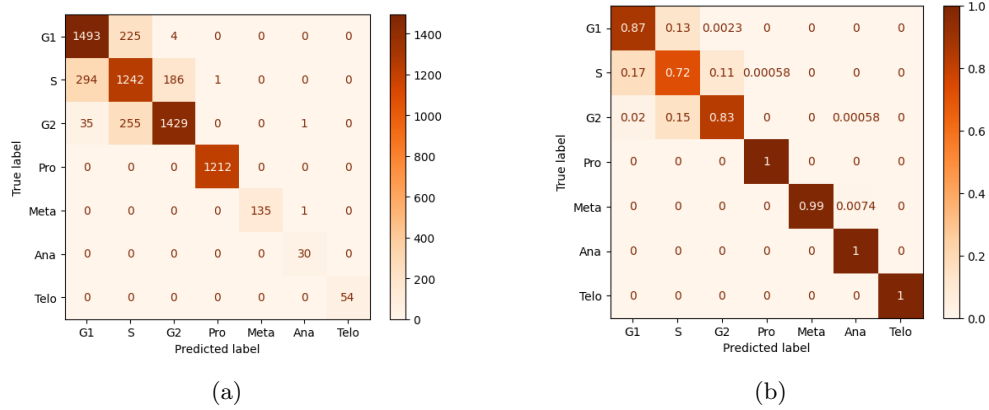



Fig. 6: a) Confusion matrix of the classification of the dataset using the WGAN-GP data augmentation technique. b) Confusion matrix normalized of the classification of the dataset using the WGAN-GP data augmentation technique.

Table 2 showcases improvements in most phases in terms of metrics, unlike the imbalanced dataset, for both the methodology proposed by Jin et al. and the proposed CNN model. The results of our model, in particular, are superior, suggesting that the utilization of a conventional CNN model can yield classification results similar to or even better than other deep learning architectures. 

Rana et al. conducted a study in which they trained a ResNet using images generated through the combination of data augmentation techniques WGAN-div + mixup. To assess the performance of our CNN model in this work, we relied upon the methodology proposed in [13]. The proposed CNN was trained using data generated through the mentioned augmentation techniques, achieving superior performance. This contrasts with the approach taken in [7], highlighting the model's strong performance

Table 2: Class-wise comparison between the proposed model and Jin et al. using the dataset with WGAN-GP data augmentation and oversampling in the G1 stage.

Phase	Precision		Recall		F1	
	Jin et al.'s model	Proposed model	Jin et al.'s model	Proposed model	Jin et al.'s model	Proposed model
G1	0.8181	0.8194	0.8490	0.8670	0.8333	0.8426
S	0.6700	0.7213	0.6918	0.7208	0.6808	0.7210
G2	0.8456	0.8826	0.7895	0.8308	0.8166	0.8559
Prophase	0.9934	0.9992	0.9909	1.0000	0.9922	0.9996
Metaphase	0.8125	1.0000	0.9559	0.9926	0.8784	0.9963
Anaphase	1.0000	0.9375	0.0667	1.0000	0.1250	0.9677
Telophase	1.0000	1.0000	1.0000	1.0000	1.0000	1.0000
Weighted Average	0.8210	0.8490	0.8184	0.8481	0.8174	0.8481

both on data without the application of augmentation techniques and on data with augmentation.

In the confusion matrix of the Figure 7, a notable scarcity of false positives and false negatives is evident. Specifically focusing on classes associated with mitosis, a virtually flawless classification is achieved, thanks to the implementation of data augmentation techniques. It is crucial to consider that, superficially, mitotic states may exhibit variations, underscoring the importance of differentiation through the inclusion of more examples.

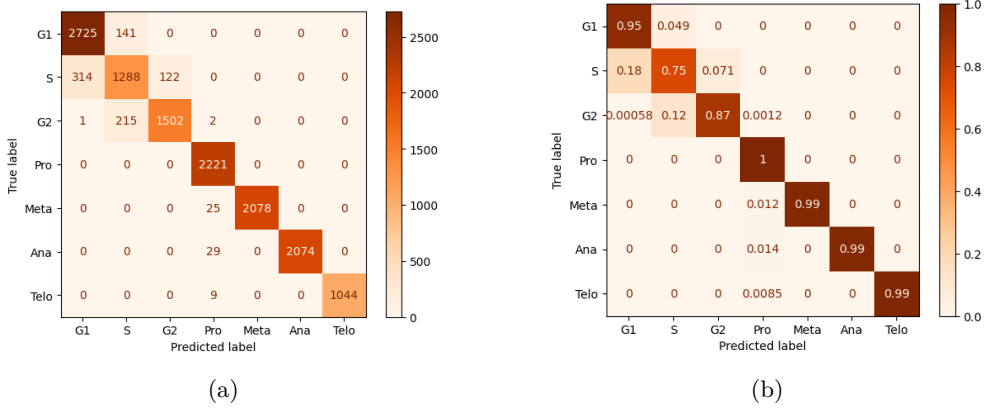


Fig. 7: a) Confusion matrix of the classification of the dataset using the WGAN-GP data augmentation technique. b) Confusion matrix normalized of the classification of the dataset using the WGAN-GP data augmentation technique.

In general, we can affirm that the developed model, fueled by examples provided by a WGAN-div, demonstrated superior performance. In Table 3, a comparison with the methodology proposed in [13]. is observed, focusing specifically on the F1 metric, where the algorithm shows good results in the majority of cell cycle states. With this, we can confirm that the proposed model enhances its efficiency by incorporating additional data.

Table 3: Class-wise comparison between the proposed model and Rana et al. [15] using the dataset with WGAN-div data augmentation and *mixup*.

Phase	Rana et al.'s model	Proposed model
G1	0.9300	0.9280
S	0.7500	0.7648
G2	0.8400	0.8983
Prophase	0.9200	0.9856
Metaphase	0.5700	0.9940
Anaphase	1.0000	0.9931
Telophase	1.0000	0.9951
Weighted Average	0.8600	0.9372



Target area 4

4 Conclusion

This project successfully achieved the classification of the 7 states in the cycle of a cancerous cell. It was demonstrated that a standard CNN model is capable of effectively classifying the phases of the cell cycle even in an imbalanced dataset. The efficiency of the CNN model is enhanced by applying data augmentation techniques. Phases of the cell cycle, which may be challenging for the human eye to observe, can be accurately classified using a deep learning model. Additionally, data augmentation techniques prove invaluable when a dataset lacks a sufficient number of images per class. This approach allows for a more robust training of the model, resulting in improved performance when assessing the model's accuracy with diverse data.



Acknowledgments. Edgar F. Duque-Vazquez thanks the Mexican National Council on Humanities, Sciences and Technology (CONAHCYT) for the scholarship grant 1081409.

Target area 5



Declarations

References

- [1] Caglar, H.O., Biray Avci, C.: Alterations of cell cycle genes in cancer: unmasking the role of cancer stem cells. *Molecular biology reports* **47**, 3065–3076 (2020)
- [2] Coffman, J.A.: Cell cycle development. *Developmental cell* **6**(3), 321–327 (2004)
- [3] Needham, D.: Possible role of cell cycle-dependent morphology, geometry, and mechanical properties in tumor cell metastasis. *Cell biophysics* **18**, 99–121 (1991)
- [4] FANG, H.-S., LANG, M.-F., SUN, J.: New methods for cell cycle analysis. *Chinese Journal of Analytical Chemistry* **47**(9), 1293–1301 (2019) [https://doi.org/10.1016/S1872-2040\(19\)61186-2](https://doi.org/10.1016/S1872-2040(19)61186-2)
- [5] Roukos, V., Pegoraro, G., Voss, T.C., Misteli, T.: Cell cycle staging of individual cells by fluorescence microscopy. *Nature protocols* **10**(2), 334–348 (2015)

- [6] Narotamo, H., Fernandes, M.S., Moreira, A.M., Melo, S., Seruca, R., Silveira, M., Sanches, J.M.: A machine learning approach for single cell interphase cell cycle staging. *Scientific Reports* **11**(1), 19278 (2021)
- [7] Jin, X., Zou, Y., Huang, Z.: An imbalanced image classification method for the cell cycle phase. *Information* **12**(6), 249 (2021)
- [8] Jose, A., Roy, R.i.-e.j., Stegmaier, J.: Weakly-supervised temporal segmentation of cell-cycle stages with center-cell focus using recurrent neural networks. In: *BVM Workshop*, pp. 212–219 (2023). Springer
- [9] Jose, A., Roy, R., Eschweiler, D., Laube, I., Azad, R., Moreno-Andrés, D., Stegmaier, J.: End-to-end classification of cell-cycle stages with center-cell focus tracker using recurrent neural networks. In: *ICASSP 2023-2023 IEEE International Conference on Acoustics, Speech and Signal Processing (ICASSP)*, pp. 1–5 (2023). IEEE
- [10] Narotamo, H., Fernandes, M.S., Sanches, J.M., Silveira, M.: Interphase cell cycle staging using deep learning. In: *2020 42nd Annual International Conference of the IEEE Engineering in Medicine & Biology Society (EMBC)*, pp. 1432–1435 (2020). IEEE
- [11] Rappez, L., Rakhlin, A., Rigopoulos, A., Nikolenko, S., Alexandrov, T.: Deepcycle reconstructs a cyclic cell cycle trajectory from unsegmented cell images using convolutional neural networks. *Molecular systems biology* **16**(10), 9474 (2020)
- [12] Eulenberg, P., Köhler, N., Blasi, T., Filby, A., Carpenter, A.E., Rees, P., Theis, F.J., Wolf, F.A.: Reconstructing cell cycle and disease progression using deep learning. *Nature communications* **8**(1), 463 (2017)
- [13] Rana, P., Sowmya, A., Meijering, E., Song, Y.: Imbalanced cell-cycle classification using wgan-div and mixup. In: *2022 IEEE 19th International Symposium on Biomedical Imaging (ISBI)*, pp. 1–4 (2022). IEEE
- [14] Rana, P., Sowmya, A., Meijering, E., Song, Y.: Data augmentation for imbalanced blood cell image classification. *bioRxiv*, 2022–08 (2022)
- [15] Gulrajani, I., Ahmed, F., Arjovsky, M., Dumoulin, V., Courville, A.C.: Improved training of wasserstein gans. *Advances in neural information processing systems* **30** (2017)
- [16] Wu, J., Huang, Z., Thoma, J., Acharya, D., Van Gool, L.: Wasserstein divergence for gans. In: *Proceedings of the European Conference on Computer Vision (ECCV)*, pp. 653–668 (2018)
- [17] Zhang, H., Cisse, M., Dauphin, Y.N., Lopez-Paz, D.: mixup: Beyond empirical risk minimization. *arXiv preprint arXiv:1710.09412* (2017)

- [18] Rijsbergen, C.: Information retrieval 2nd ed buttersworth. London, 115 (1979)